Structures, solvation forces and shear of molecular films in a rough nano-confinement

Jianping Gao, W.D. Luedtke and Uzi Landman

School of Physics, Georgia Institute of Technology, Atlanta, GA 30332-0430, USA

Investigations of surface roughness effects on the structure, dynamics and rheology of a molecular fluid (hexadecane) confined between solid (gold) surfaces, through the use of large-scale molecular dynamics simulations, reveal a remarkable sensitivity to the confining surface morphology. A most significant reduction of the ordering propensity is found in films confined by stationary rough surfaces with a consequent strong suppression of solvation forces and the development of liquid-like dynamic and response characteristics. When the rough-surface boundaries are set in motion at a high shear rate, the interfacial layers of the film stick to the adjacent solid boundaries, resulting in partial slip inside the film with the development of shear stress in the viscous molecular fluid, unlike the case of atomically flat crystalline boundaries where slip of the confined film at the boundaries is accompanied by vanishingly small shear stress in the film. These results are discussed in the context of the effect of roughness on the boundary conditions used in modeling fluid flow past surfaces, and they suggest that morphological patterning of surfaces could provide ways for controlled modifications of frictional processes in thin-film lubricated nanotribological systems.

Keywords: molecular dynamics simulations, roughness effects, thin-film rheology, confined fluids, solvation forces, shear flow, boundary lubrication, nanotribology

1. Introduction

In a recent series of papers [1–3] we have investigated the origins and systematics of solvation forces in thin films made of molecules of different sizes and molecular architectures (that is, spherical molecules, straight-chain alkanes of different length (n-hexadecane, n-$C_{16}H_{34}$, and n-tetracosane, n-$C_{24}H_{50}$) and a branched alkane (squalane, 2,6,10,15,19,23-hexamethyltetracosane)), confined by atomically structured flat solid surfaces modeled as the close-packed planes of Au(111). In these studies we have shown through extensive grand-canonical molecular dynamics simulations [1], that all the above films exhibit density-layering normal to the confining surfaces, and that for the films made of spherical or straight-chain alkanes the solvation force (that is, the normal force acting on the confining boundaries) varies as a function of the distance between the confining solids (i.e., gap-width) in an oscillatory manner (with a period approximately equal to the width of the molecules), while for the branched alkane such solvation force oscillations are significantly weakened (for an experimental study of the solvation force in squalane films see ref. [4]). These trends were shown to be reflected in the response of the films to a decrease in the gap-width, with that found for the spherical and straight-chain alkanes being of step-like character, that is, squeeze-flow involving stress accumulation in the molecular film until a critical value is reached, resulting in a sudden expulsion of about a layer-worth of molecules from the confinement into the surrounding reservoir. In contrast, for the case of the branched alkane film changes in the width of the confinement were found to be accompanied by continuous (liquid-like) outflow (expulsion) of molecules from the confined

region. Furthermore, the patterns found for the solvation forces were shown to be portrayed in the behavior of the free-energy of the films (i.e., potential and entropic contributions) as a function of the width of the confinement, with that of the branched alkane exhibiting a smooth variation, in contrast to the oscillatory character of the free-energy calculated for the spherical and straight-chain alkanes.

The high sensitivity of the structural, dynamic and rheological properties of confined films to (small) variations in the gap-width revealed by the above simulations, led to the development [5] of a method for control of friction in lubricated junctions via small amplitude (of the order of one angstrom) oscillations of the gap-width applied in the direction normal to the shear plane. Such directional oscillations frustrate ordering processes in the confined film, and when applied with the appropriate frequency (which is determined by relaxation times characteristic of the lubricating material) they have been shown (theoretically [5], as well as in experiments [6] aimed at verification of the theoretical predictions) to influence the sliding dynamics (that is, transform stick–slip motion into smooth sliding) and reduce significantly the frictional resistance.

Molecular dynamic simulations of the tribological, rheological, and viscoelastic properties of confined films in equilibrium and under shear conditions, have been performed to date, almost exclusively, for atomically flat (smooth) crystalline confining solid boundaries (for reviews [7,8], and for exceptions see, e.g., [9–11][1]); the variation along the surface plane of the interaction potential between the lubricating film molecules and the surface atoms is often re-

---

[1] For Monte Carlo simulations of roughness effects on the properties of confined fluid films see [12].

ferred to as the surface corrugation, and it depends on the crystalline face exposed. Shearing of fluids in confined (lubricated) junctions can be simulated (as well as studied in laboratory experiments [13]) via attachment of a (horizontal) spring (of force constant k_s) to one of the confining solids (say the top one) with the free end of the spring translated with a constant velocity (v), or equivalently by attaching such springs to both of the confining solids and translating them in opposite directions with velocities $v/2$ and $-v/2$. For stiff springs (i.e., $k_s \to \infty$) the confining solid surfaces are set in motion at a relative constant velocity v with respect to each other, while for a finite k_s stick–slip phenomena may appear for $v < v_c$, where v_c is a critical velocity above which a transition to steady motion occurs [14].

However, at shear rates of interest in modern tribological systems [15] (lubricated films of the order of 1 to 2 nm with sliding velocities of $\sim$1–10 m/s, i.e., shear rates of 10^9–10^{10} s^{-1}), it is commonly found in simulations [16–19][2] employing flat close-packed (atomically structured) solid surfaces, that for large k_s and for chain molecules (as well as spherical molecules whose size (diameter) is incommensurate with the interatomic distance in the confining solid surfaces) the motion of the surfaces is accompanied by slip of the confined film at the film–solid interface. In this study we show through large-scale molecular dynamics simulations that when the confining solid surfaces are rough such boundary-slip of the confined film (n-hexadecane) is highly suppressed even for rough-surface morphologies characterized by atomic-scale height variations. Furthermore, our investigations reveal remarkable sensitivity of the structural, dynamic and rheological properties of confined molecular films to the surface morphology, both under static conditions (that is when the solid boundaries are stationary) and under shear (that is when the solid boundaries are in relative motion with repect to each other), resulting from frustration of ordering in the molecular film in rough surface confinements.

For the static case the reduced ordering propensity of the rough-surface confined film (compared to that of the film confined under similar conditions by flat solid surfaces) is exhibited by significant obliteration of the development of density-layered (stratified) structures in the film, with consequent strong suppression of the development of solvation forces, the disappearance of solvation force oscillations, and the emergence of liquid-like dynamic and response characteristics (that is higher molecular mobilities, and continuous expulsion of molecules from the confined region in response to reduction of the gap-width). When the rough-surface boundaries are set in motion (at a high shear rate) the above characteristics of the confined film maintain, with the interfacial layer of the film sticking to the adjacent solid boundaries (on the two sides of the confinement gap), resulting in partial slip inside the film and development of shear stress in the viscous molecular fluid (unlike the case

of flat boundaries where the confined film slips at the solid boundaries resulting in a vanishingly small shear stress in the film).

The above results are of importance for understanding the behaviour of lubricating films under high confinement conditions, and they allow investigations (both molecular dynamics simulations and experimental studies) of thin-film tribology and rheology at extremely high shear rates that are of relevance to current technologies. Additionally, the results obtained in our simulations for the dynamics and rheology of fluid films sheared between rough boundaries are of interest for studies pertaining to the effect of roughness on the boundary conditions used in the context of hydrodynamical approaches to such film-flow problems, including roughness effects on the effective slip-length [20–25].

In section 2 we describe the simulation method used in this study, and give pertinent details of the interaction potentials employed by us and the procedure which we developed for creation of rough solid surfaces. The results of our investigations for both static and shear conditions, are presented in section 3, and a summary of our results is given in section 4.

2. Method

2.1. The grand-canonical molecular dynamics method

In this investigation we used the grand-canonical molecular dynamics (GCMD) simulation method developed by us previously [1,2] for investigations of the properties of confined systems. In the GCMD the simulation cell (of lengths H_x, H_y, and H_z along the cartesian coordinate axes) contains both liquid molecules and solid blocks, with periodic boundary conditions replicating the entire simulation cell in all three directions. The solid blocks are of finite size in the x-direction, and the distance separating the two surfaces of the solid blocks in the z-direction defines a gap of width D; in our simulations the solid surfaces forming the gap in the middle of the cell are modeled as flat gold (111) planes or as rough gold surfaces (see below). In the y-direction, the solid blocks extend throughout the whole simulation cell and in simulations of shear motion the solids are translated along the y-direction. In the current study, the lengths of the solid blocks in the x- and y-directions are, respectively, 196 and 204 Å for the rough confinement case, and both are 200 Å in length for the flat-surface confinement.

The rest of the space in this three-dimensional simulation cell (i.e., the space not occupied by the solids) is filled with fluid molecules. With this arrangement two regions of the alkane fluid can be distinguished. Inside the gap (i.e., between the two solid surfaces) the alkane molecules are confined as a thin film with a thickness D (ranging in the present study between 10 and 40 Å), and the size of the cell in the x-direction is taken to be sufficiently large so that the molecules in the regions outside the interfacial solid confinement can exhibit bulk liquid behavior (in the present

---

[2] See review and discussion in [8].

study $H_x \geqslant 300$ Å). The size of the cell in the x-direction H_x is allowed to vary dynamically through the use of the constant pressure molecular dynamics method [26]; in our simulations the hydrostatic pressure in the reservoirs, determining the magnitude of H_x, was taken to be 1 atm (on the scale of all other stresses in the system this represents a vanishingly low pressure). In the y-direction the length of the simulation cell (and that of the solid surfaces) is held constant (i.e., 204 and 200 Å for the rough and flat confinements, respectively), while the length of the computational cell in the z-direction (i.e., normal to the solid surfaces) is varied to give the desired film thickness in the gap; denoting the thickness (i.e., length in the z-direction) of each solid block by d_s (of the order of 15 Å in our present simulations) the length of the simulation cell in the z-direction is given by $H_z = 2d_s + D$.

We remark that the dimensions of the solid surfaces confining the liquid film are much larger in the present simulations than those used in previous studies; this is of particular importance for simulations involving rough surfaces, where a faithful representation of the statistical distribution of the surface heterogeneous morphology is essential. Consequently, the number of particles (atoms of the solid blocks and hexadecane molecules of the fluid, each containing 16 united-atom segments) treated in our simulations is rather large[3], and efficient simulations were enabled through parallelization of the GCMD computer program (using a spatial decomposition algorithm).

In this study the alkane molecules were treated dynamically, while in most of the simulations the gold atoms of the solid substrates were kept in their relaxed equilibrium positions (we have verified that treating the solids dynamically does not affect our results). The equations of motion were solved by the Verlet algorithm with an integration time step of 3 fs, with the temperature of the system controlled via the method described in ref. [27] (when equilibrium is reached no temperature control is necessary); the temperature in the simulations was taken as 350 K, which allows the systems to equilibrate in a reasonable amount of computing time.

2.2. Interaction potentials

The alkane molecules were represented in our simulations by the united-atom model, without rigid constraints. The intramolecular potentials include bond stretching, bond-angle bending, torsion angle, and Lennard-Jones (LJ) interactions between all segment-pairs separated by more than three bonds. The bond stretching is represented

by a stiff linear spring, with the bond force constant reduced by a factor of 4 from its realistic value to facilitate computations with an increased time step (this has no effect on our results). The angle bending, torsional potentials, and LJ potentials describing the intra- and inter-alkane interactions are the same as those used described in [28]. The interactions between the alkane segments and the gold atoms of the solid substrates are described by a LJ potential with parameters fitted to experimental desorption data (see [29,30]), and in simulations where the dynamics of the solids is included the interactions between the gold atoms are modeled by the many-body embedded-atom-method (EAM) potentials [31].

2.3. Preparation of rough surfaces

To prepare atomically rough surfaces of the confining solids we developed the following procedure:

(i) First, an equilibrated (at 350 K) solid gold slab (replicated in the x- and y-directions through the use of periodic boundary conditions) made of eight layers treated dynamically and two additional bottom static layers stacked as a face-centered-cubic crystalline solid and exposing the (110) surface, was heated up to a temperature of 1100 K resulting in melting of the top few layers of the solid.

(ii) After equilibration of the system at 1100 K it was cooled to 350 K in 200 ps and then equilibrated at 350 K for an additional period of 300 ps. This procedure was applied separately to both the top and bottom confining slabs in order to create two uncorrelated rough surfaces.

3. Results

3.1. Surface roughness

A visual impression of the rough surfaces obtained through the preparation procedure described in the previous section may be gained from inspection of figure 1 where side views of the confining solids are shown (with an empty gap in figure 1(a) and a thin slice through the fluid-filled gap in figure 1(b)); note that the nature of the topography of these (statistically) rough surfaces differs from the (periodically) corrugated structure of atomically flat crystalline surfaces. The degree of effective roughness of the surfaces has been quantified as follows:

(i) The surfaces were scanned by a sphere of radius 1.97 Å (that is, equal to half of the size parameter, $\sigma(\mathrm{CH_2-CH_2})$), in the LJ potential describing the interaction between the (united-atom) alkyl segments of the alkane molecule), and at each point (x_i, y_i), lying on a two-dimensional grid with 1 Å spacing in the x- and y-directions, the height z (measured from the bottom layer of the solid slab), where the interaction between the scanning-ball and the

---

[3] In these simulations, the total number of atoms in the solid blocks are 89,600 for the flat-surface confinement (with eight layers in each block stacked as a face-centered-cubic solid in the $\langle 111 \rangle$ direction), and for the rough-surface confinement the total number of solid atoms is 68,000 (starting before preparation of the rough-surface, see text, from ten layers in each block, eight of them treated dynamically and two underlying static layers, stacked as a fcc solid in the $\langle 110 \rangle$ direction). The total number of hexadecane molecules varies in our simulations between about 5800 and 3350 depending on the gap-width, with about 350 molecules per layer in the confined region.
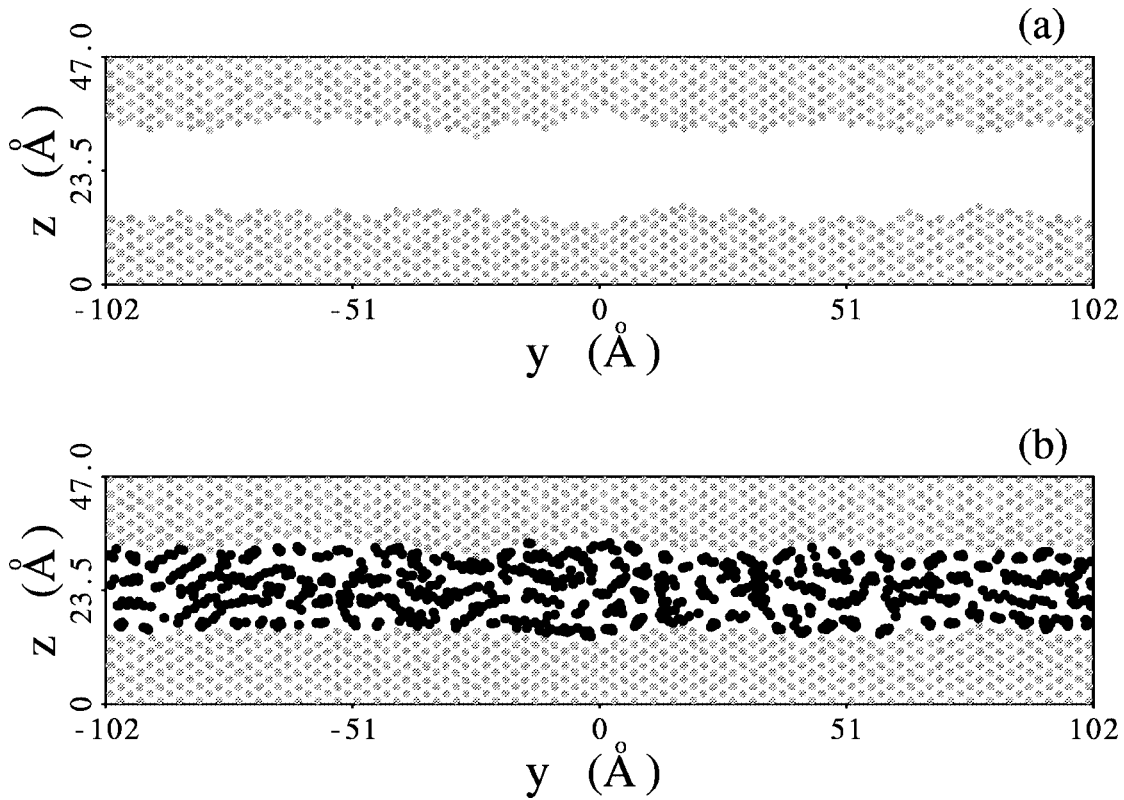
Figure 1. Side view (along the x-axis) of a slice (about 9.2 Å thick) lying in the y–z plane and passing through the center of the simulation cell; the shown atomic configuration corresponds to the rough-surface confinement with an average gap-width $\overline{D} = 20$ Å. The gray dots represent gold atoms in the confining solid blocks and the black dots represent alkane segments. (a) Solid blocks with an empty gap, and (b) solid blocks with a confined n-hexadecane film.

solid gold surface changed from being attractive to becoming repulsive, was recorded. The height distribution $P(z - \bar{z})$ (normalized by the number of scanning points), with $\bar{z}$ denoting the average surface height, is shown in figure 2(a). The $P(z - \bar{z})$ distribution exhibits three main peaks, with the two side peaks centered at ± 1.4 Å corresponding to surface sites above and below $\bar{z}$ (note that the interlayer spacing in crystalline gold in the $\langle 110 \rangle$ direction is about 1.4 Å); the root-mean-square deviation of this distribution eqauls 1.1 Å. The corresponding distribution, $P(D - \overline{D})$, of the gap-widths (D) with reference to $\overline{D} = \bar{z}_{\mathrm{u}} - \bar{z}_{\mathrm{b}}$, where $\bar{z}_{\mathrm{u}}$ and $\bar{z}_{\mathrm{b}}$ are, respectively, the average surface heights of the upper and bottom solid slabs, is displayed in figure 2(b). $P(D - \overline{D})$ shows that the variation in gap-width between the confining surfaces varies by up to ± 4.0 Å with a root-mean-square deviation of ± 1.6 Å about $\overline{D}$.

(ii) Using the recorded height values (z) determined as described above, we evaluated the lateral height–height correlation function $C(R) = \langle z(R)z(0) \rangle$, where the angular brackets denote an average over the origins of R (on the (x_i, y_i) grid) and $R < 100$ Å (i.e., less than half the length of the confining solid surface in the x- and y-directions). From an exponential fit ($\sim \mathrm{e}^{-R/l_{\mathrm{c}}}$) to $C(R)$ we obtained a correlation length $l_{\mathrm{c}} = 6.9$ Å, which characterizes the roughness of the surfaces created by the procedure debribed in section 2.3 as short-ranged; we also note that flat regions

extending for more than several angstroms are rarely found on these rough surfaces.

3.2. Equilibrium structures and solvation forces

To explore the effect of the surface roughness on the structure and energetics of the confined molecular liquid (hexadecane, n-$\mathrm{C_{16}H_{34}}$) the confined system in contact with the reservoir was equilibrated first, at a temperature $T = 350$ K, for a relatively large gap-size $\overline{D} = 32$ Å (~ 8 molecular widths); here and in the following we use $\overline{D}$ to denote the gap-width in both the rough surface (RS) and flat-surface (FS) confinements. Starting from this initial equilibrated system the gap-width was reduced in small increments with full equilibration performed after each variation of the gap-width. Such simulations were performed for the RS and FS solid confinements.

In figure 3 we display the forces on the confining substrates recorded in both simulations, exhibiting an expected "solvation force" oscillatory pattern for the flat-surface (FS) confinement (dashed line), while no such oscillations are found for the rough-surface (RS) confinement which exhibits instead a vanishing solvation force up to $\overline{D} \approx 18$ Å with the development of very small repulsive forces for smaller gap-widths (see solid line). The density profiles of the confined fluid for the two systems plotted in figure 4 as a function of distance (z) across the confining gap
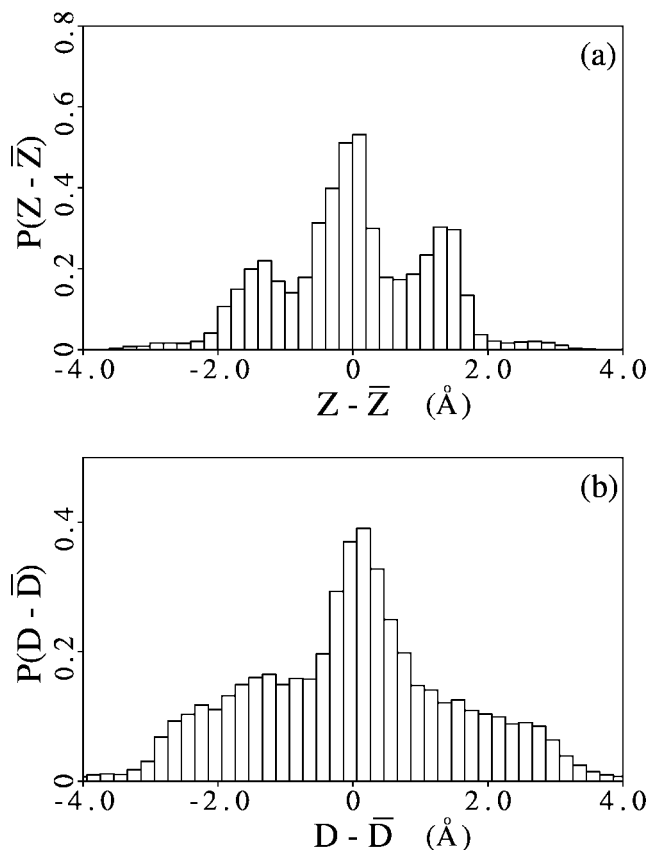
Figure 2. (a) Height-distribution of the rough gold surfaces, $P(z - \bar{z})$ versus $z - \bar{z}$ (where $\bar{z}$ is the average surface height). The root-mean-square deviation of the distribution equals 1.1 Å. (b) The gap-width distribution, $P(D - \overline{D})$ versus $D - \overline{D}$ (where $\overline{D}$ is the average gap-width), corresponding to the height distribution shown in (a). The root-mean-square deviation of this distribution equals 1.6.
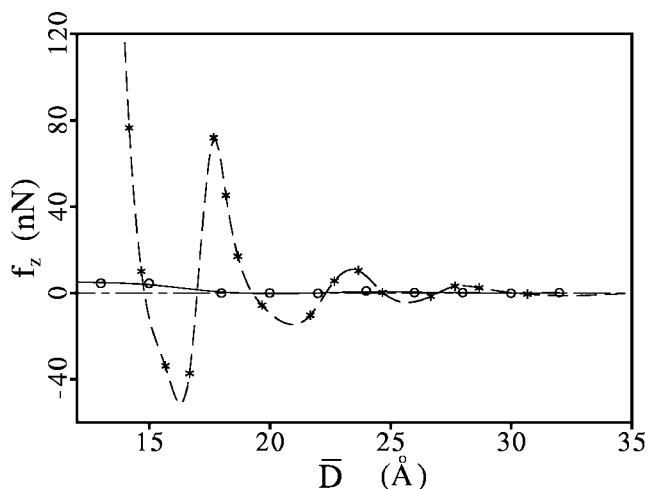

Figure 3. Solvation forces, f_z, plotted vs. the (average) gap-width, $\overline{D}$, for hexadecane confined by solid (gold) rough and flat surfaces. The open circles connected by a solid line correspond to the rough-surface confinement, and the stars connected by a dashed line correspond to the flat-surface confinement. For the flat-surface confinement the repulsive force rises sharply for $\overline{D} < 15$ Å, with $f_z = 174$ nN at $\overline{D} = 13.7$ Å (not shown in the figure). The conversion factor for our system, between the solvation force, f_z, and the normal pressure, τ_{zz}, is 1 nN = 2.5 MPa.

for selected values of $\overline{D}$, exhibit density-layering, which is much sharper and well-defined for the FS confinement (figure 4(b)); note in particular the sharply defined interlayer regions for the FS confinement in contrast to the RS confinement case (compare figure 4(b) with figure 4(a), respectively). Indeed, visual inspection, as well as analysis of order parameters, show a high degree of intermolecular inplane order with a very small degree of interlayer interdigitation in the FS confinement case, and a markedly smaller degree of such order accompanied by interlayer interdigititation found for the molecular film in the RS confinement.

The different nature of the molecular films confined by the flat and rough surfaces is illustrated in figure 5 via comparison of the free-volume fraction ($f_v = v_f/v_t$ where v_t is the total volume of the confined liquid region), calculated for the two systems at various gap-widths; the free-volume v_f was evaluated by dividing the systems into a cubic grid (1 Å × 1 Å × 1 Å) and summing the volumes of all the grid boxes whose centers do not lie inside any molecular segment (defined as a sphere of radius 1.97 Å, i.e., $0.5\sigma(CH_2-CH_2)$) or inside any surface gold atom (defined by a sphere of radius 1.32 Å, i.e., half of the size-parameter corresponding to a gold atom, used in the LJ potential describing the interaction between a gold atom and a molecular segment). In both systems f_v is found to be smaller inside the confinement than in the bulk liquid (f_v(bulk) $\approx 1/3$). However, in the FS confinement the variation of f_v with $\overline{D}$ is non-monotonic (dashed line) exhibiting local minima for gap sizes corresponding to well-layered film configurations (see figure 4(b)) which become deeper (that is lower f_v) as $\overline{D}$ decreases, while in the RS confinement the f_v exhibits a slow (smooth) monotonic decrease with $\overline{D}$, and the f_v value for a given gap-width is larger in the RS case than in the corresponding FS confinement (except near values of $\overline{D}$ corresponding to intermediate configurations between well-layered states of the film in the FS confinement).

The larger values of f_v in the RS confinement and its smooth monotonic variation with size (see solid line in figure 5) suggest frustration of ordering of the fluid, and liquid-like structure and response characteristics of the confined film, correlating with the monotonic smooth pattern exhibited for the RS confinement in figure 6, where we display the number of molecular segments in the confinement, n_{cfn}, as a function of the gap-width [1–3]; such smooth monotonic dependence of n_{cfn} on the gap-width is characteristic of squeeze flow of liquids. On the other hand, the local minima in f_v and the step-like variation of n_{cfn} found for the FS confinement (see dashed line in figure 6, with the height of each step corresponding to approximately 350 hexadecane molecules, i.e., a layer-worth of molecules in the confined region) correlate with the development of load-supporting ordered states, with the response to shrinking of the gap-width characterized by transitions between one well-layered structure to another (with the number of liquid layers reduced by one in the latter) that occur through a mechanism of stress accumulation in the film and sub-
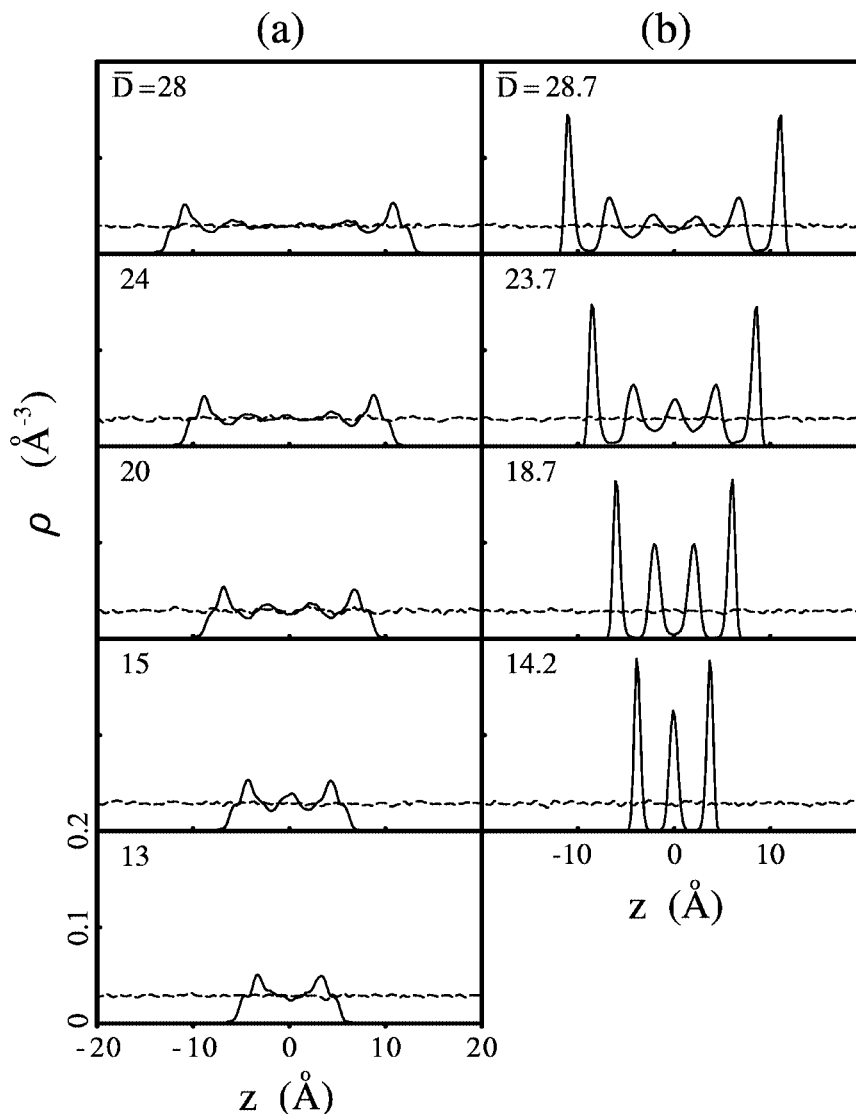
Figure 4. Hexadecane segmental density profiles, plotted as a function of distance along the axis normal to the solid planes (z) for selected values of the gap-widths $\overline{D}$. The solid lines correspond to the film in confined region, and the dashed lines are calculated in the bulk reservoir region. (a) Rough-surface confinement, and (b) flat-surface confinement.

sequent yield accompanied by abrupt expulsion of about a layer-worth of molecules from the confined region into the bulk reservoir [1–3].

Additional information pertaining to the different dynamical nature of the films in the FS and RS confinements is provided by their segmental two-dimensional diffusion coefficients D_{xy}. Indeed, while for the FS confinement with $\overline{D} = 18.7$ Å we find $D_{xy} = 1.2 \times 10^{-6}$ cm^2/s, a higher value of $D_{xy} = 4.7 \times 10^{-6}$ cm^2/s is calculated for the film with $\overline{D} = 20$ Å in the RS confinement; note that both values are much smaller than that corresponding to the molecular liquid in the bulk reservoirs where $D_{xy} = 2.3 \times 10^{-5}$ cm^2/s.

3.3. Shear and confined-film rheology

Starting from an equilibrated state of the confined film, it is subjected to shear where the confining solids are moved at constant velocity (i.e., an infinitely stiff pulling spring)

in opposite directions along the y-axis (i.e., $\pm v/2$) with the gap-width held constant. Such simulations of shear motion were performed by us for both the FS confinement (for gap-widths corresponding to well-ordered layered configurations), and for similar gap-widths ($\overline{D}$) of the RS confinement.

In figure 7 we display the time-variation of the average displacement Δ of molecular segments in various regions of the film for the 4-layer FS confinement ($\overline{D} = 18.7$ Å) and for the RS confinement ($\overline{D} = 20$ Å), sheared with a relative velocity $v = 1$ m/s (corresponding to a shear rate of about 0.5×10^9 s^{-1}); the regions in the film (denoted as 1 through 4 in figure 7) correspond to the layers in the FS (see figure 4(b) at $\overline{D} = 18.7$ Å) and RS (see figure 4(a) at $\overline{D} = 20$ Å) confinements. The responses to shear of the films in the two confinements differ in an essential way. Thus, while the film in the FS confinement exhibits an almost complete slip at the film-to-solid inter-
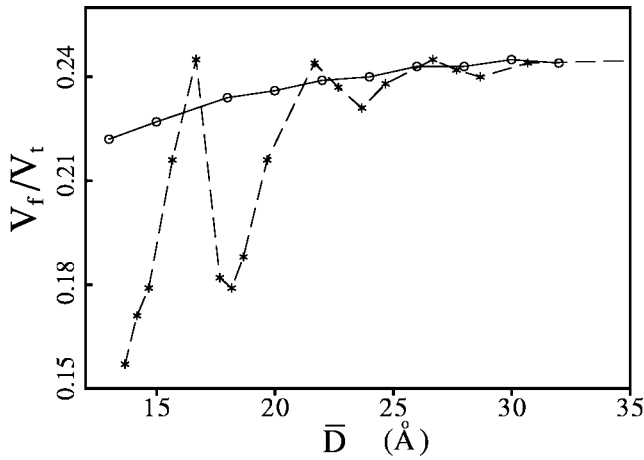
Figure 5. Free-volume fractions in equilibrated configurations of a confined hexadecane film, plotted as a function of the average gap-width $\overline{D}$. The open circles connected by a solid line correspond to the rough-surface confinement, and the stars connected by the dashed line correspond to the flat-surface confinement. Note the sharp dips occurring at gap-width values corresponding to well-layered configuration of the film in the flat-surface confinement.
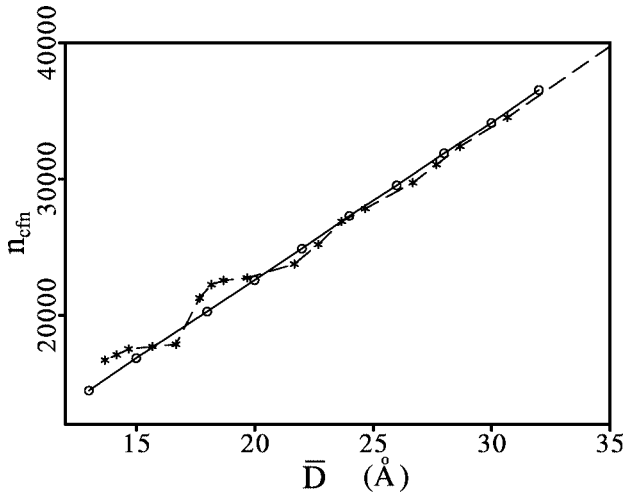

Figure 6. The number of hexadecane molecular segments in the confined region (n_{cfn}), plotted as a function of gap-width, $\overline{D}$. The open circles connected by the solid line correspond to the rough-surface confinement and the stars connected by a dashed line correspond to the flat-surface confinement. Note the step-like variation for the flat-surface confinement, with the heights of the step-rises equal to about a layer-worth of molecular segments; the number of hexadecane molecules in each layer in the confined region is about 350 which when multiplied by the number of segments in each molecule (16) yields 5600 molecular segments per layer.

face (see figure 7(a)), only the interior middle layers of the film (2 and 3 in figure 7(b)) in the RS confinement develop a finite degree of slip with the boundary layers (1 and 4 in figure 7(b)) sticking to the confining rough surfaces; the straight solid lines in figures 7 (a) and (b) describe the displacement of the confining solid boundaries (translated at a constant velocity with respect to each other).

The above differences in the dynamics of the shear flow at the boundaries are reflected in the shear stress τ_{yz} (cal-

culated for the above gap-widths from the forces exerted by the confined film on the solid boundaries), shown in figure 8 for the FS and RS confinements (left and right panels, respectively) for two relative shearing velocities, $v = 1$ m/s (in figure 8(a)) and $v = 2$ m/s (in figure 8(b)). From these results we observe that at both velocities the slip of the boundary layer of the film in the FS confinement is reflected in small values of τ_{yz} portraying the inability of the confined film to develop shear stress, while in the RS confinement significant shear stresses develop, increasing (by about a factor of two) as the sliding velocity is doubled (compare right panels in figure 8 (a) and (b)). At the same time the stress component in the direction normal to the boundaries (τ_{zz}) is rather high in the FS confinement (see left panels in figure 8 (c) and (d)) and it is exceedingly small for the RS one (see right panels in figure 8 (c) and (d)), correlating with the vanishing of the solvation force in the RS confinement (see figure 3).

The above observations pertaining to total slip at the interface between the confined film and the solid boundaries (and consequently vanishing of the shear stress in the molecular film), were found to maintain for other gap-widths of the FS confinement. Shear simulations of the RS confinement at other gap-widths also resulted in non-slip behaviour of the film layers in immediate contact with the solid boundaries accompanied by the the development of shear stress in the confined film (as illustrated above for the $\overline{D} = 20$ Å RS confinement), with the average value of the shear stress in the film becoming significantly larger for increased confinement (that is, smaller gap-width $\overline{D}$). From the calculated average values of $\tau_{yz}(\overline{D})$ and the shear rate $\dot{\gamma} = v/\overline{D}$ an estimate for the effective viscosity of the film in the RS confinement may be obtained as $\eta_{eff}(\overline{D}) = \tau_{yz}(\overline{D})/\dot{\gamma}$. Our simulations show that the effective viscosity increases significantly with decrease of the gap-width (i.e., higher confinement) [32][4], changing from a value of $\eta_{eff}(\overline{D} = 40$ Å$) \approx 1$ cp (at $\dot{\gamma} = 0.5 \times 10^9$ s^{-1}) to $\eta_{eff}(\overline{D} = 13$ Å$) \approx 36$ cp (at $\dot{\gamma} = 0.4 \times 10^9$ s^{-1}). For the $\overline{D} = 20$ Å film at $\dot{\gamma} = 0.5 \times 10^9$ s^{-1} (see figure 7(b), and figure 8(a)) the calculated average shear stress is 1.8 Mpa and $\eta_{eff}(\overline{D} = 20$ Å$) = 3.6$ cp, and at twice the shear rate (i.e., 1×10^9 s^{-1}, see figure 8(b)) the value of the shear stress is approximately doubled (3.7 Mpa), with the effective viscosity remaining essentially unchanged (3.7 cp); from these observations one may conclude that for this gap-width the film behaves as a Newtonian fluid. However, it is important to note that for higher confinements (that is, smaller gap-widths), and for similar shear rates as above, shear-thinning develops.

Finally, we remark that the results of our simulations for the rough surface confinement reveal an exponential relationship between the (gap-width dependent) effective viscosity (determined for a range of gap-widths, i.e., 13 Å $\leqslant \overline{D}$ $\leqslant 40$ Å) and the reciprocal of the free-volume calculated per

---

[4] For early experimental studies of the effect of gap-width on the dynamics and rheology of confined fluids, see [33].
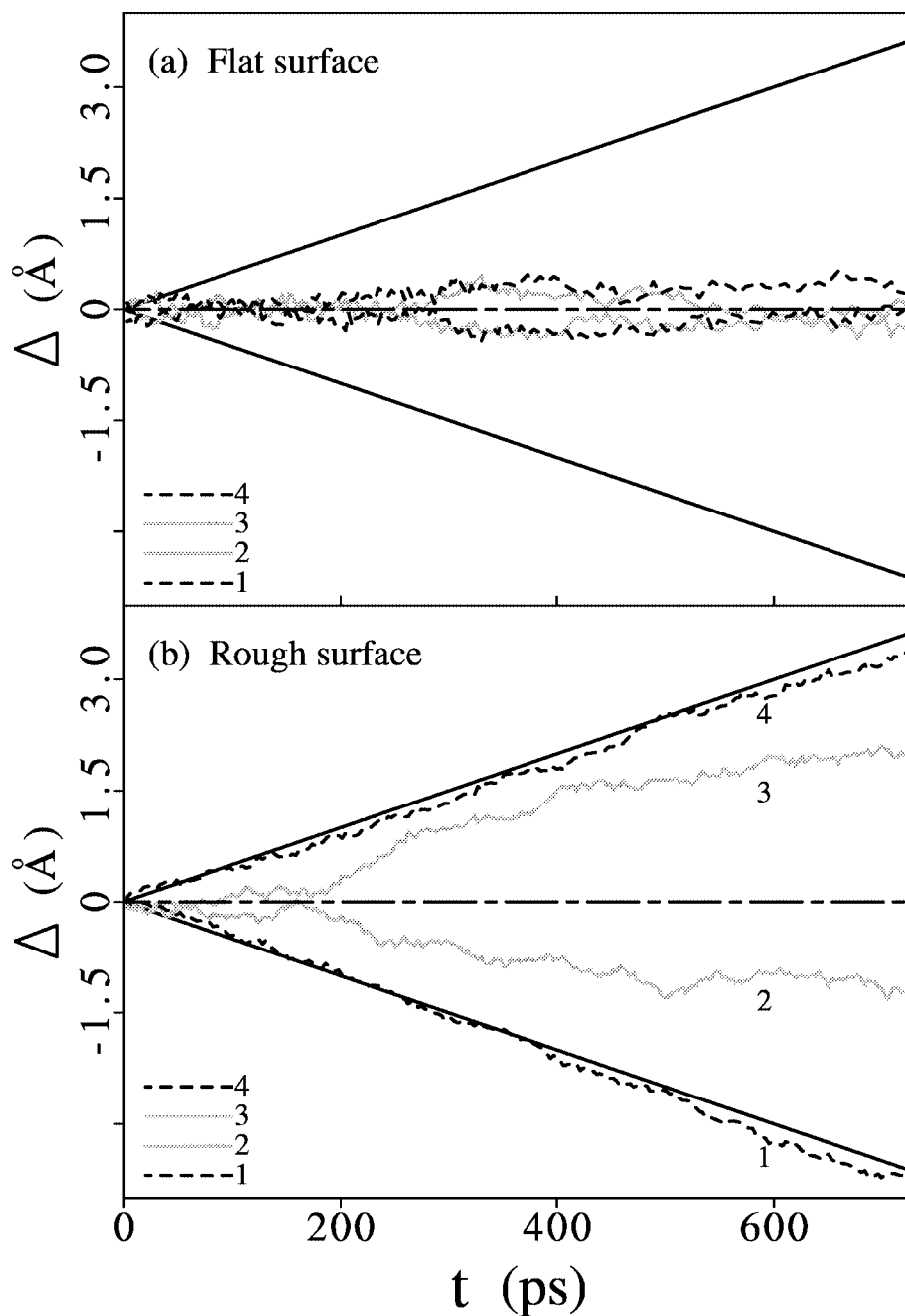
Figure 7. Average segmental displacements (Δ) for various layered regions in a confined hexadecane film, plotted vs. time during shear simulations. Results are displayed in (a) for a 4-layer film in the flat-surface confinement with $\overline{D} = 18.7$ Å, and in (b) for a film in the rough-surface confinement with $\overline{D} = 20$ Å. The confining solid blocks move at constant relative velocity of 1 m/s, and the solid straight lines correspond to the displacements of the top and bottom confining solid blocks which move in the opposite directions. The regions in the film are determined by the layer positions shown in the segmental density profiles (see figure 4(a), $\overline{D} = 20$ Å for the rough-surface confinement, and figure 4(b), $\overline{D} = 18.7$ Å for the flat-surface confinement). Regions 1 and 4 correspond to the layers of fluid next to confining solid surfaces. Regions 2 and 3 are the middle layers. Note that in the flat-surface confinement slip occurs at the interface between the solid blocks and the confined film, while in the rough-surface confinement the film boundary layers stick to the solid surfaces.

molecular segment in the confined film, i.e., Log[$\eta_{eff} (\overline{D})$] is found to be proportional to $[v_f(\overline{D})/n_{cfn}(\overline{D})]^{-1}$. A full discussion pertaining to this relationship, which has been derived through the free-volume theory [34] and used extensively in studies of disordered materials and the glass transition as well as in polymer science [35], is beyond the scope of this paper and will be given elsewhere.

4. Summary

In this paper we explored through the use of large-scale grand-canonical molecular dynamics simulations surface roughness effects on the structure, dynamics and rheology of a molecular fluid (hexadecane) confined between solid (gold) surfaces. These investigations revealed a re-
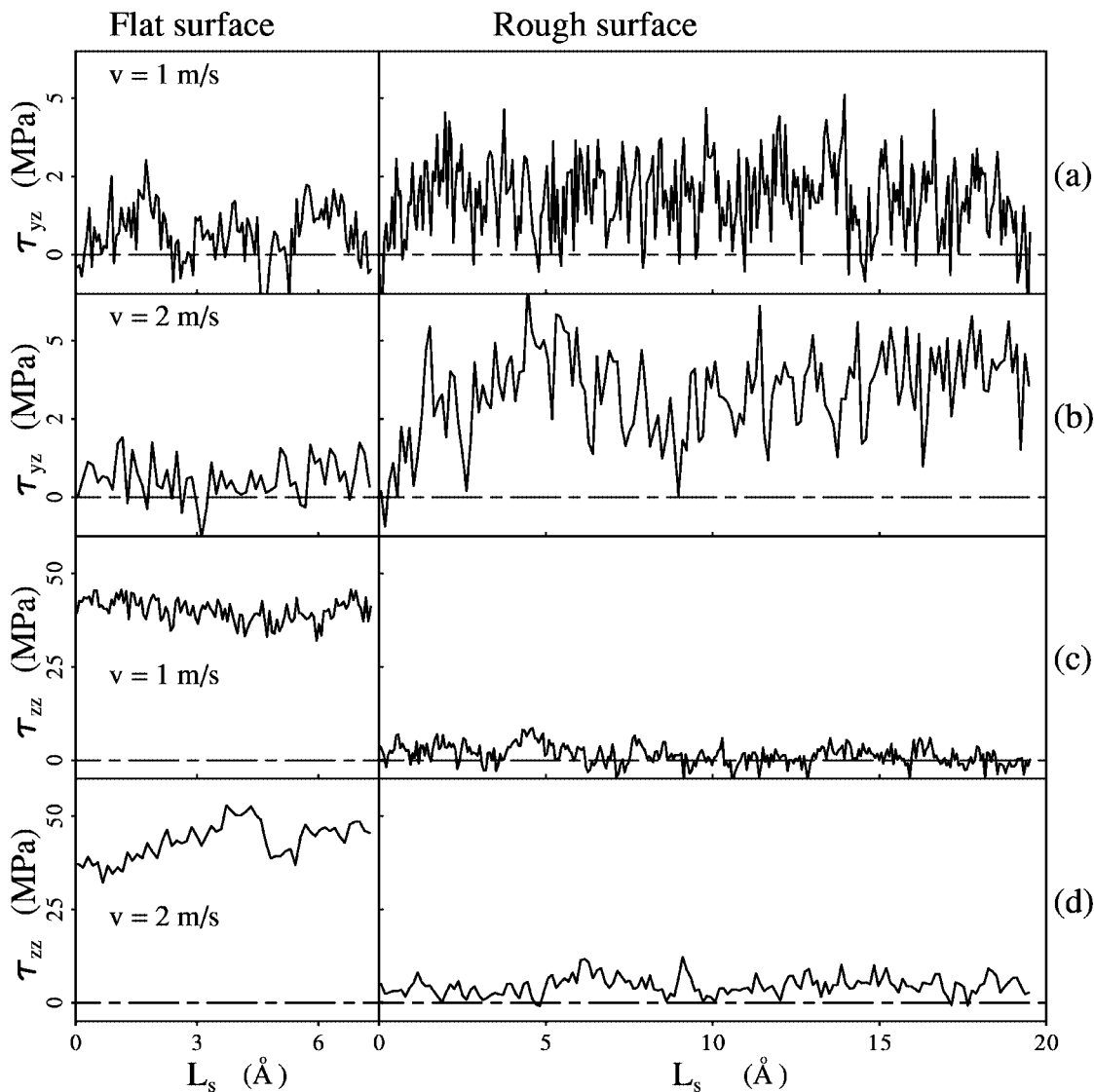
Figure 8. Shear (τ_{yz}) and normal (τ_{zz}) stresses plotted vs. relative displacement (L_s) of the confining solids during shear simulations of 4-layer confined films ($\overline{D} = 18.7$ Å and $\overline{D} = 20$ Å for the flat- and rough-surface confinements, repectively), with the boundaries translating at a relative velocity of 1 or 2 m/s. The stresses are calculated from the total force exerted on the solid surfaces by the confined films. The results for flat-surface confinement are shown on the left, and those for the rough-surface confinement are shown on the right. Note that the simulations for the FS confinement are much shorter than those for RS confinement, since steady state is reached in the former a short time after the start of the motion because of the total slip of the film at the boundary (see, figure 7(a)). The average shear stress in the film in the RS confinement, evaluated over the second half of the shearing process is 1.8 MPa for $v = 1$ m/s (see (a) right) and it essentially doubles (i.e., 3.7 MPa) for $v = 2$ m/s (see (b) right).

markable sensitivity of structural, dynamic and rheological properties of the molecular films to the confining surface morphology. Indeed, our simulations demonstrate that even a surface roughness characterized by atomic-scale height variations can modify in a most significant way the nature of fluid films confined between such surfaces, both under static conditions (i.e., when the solid boundaries are stationary) and under shear (i.e., when the solid boundaries are in relative motion with repect to each other).

For the static case the reduced ordering propensity of the rough-surface confined film (compared to that of the film confined under similar conditions by flat solid surfaces) is exhibited by significant inhibition of the development of density-layered (stratified) structures in the film

(see figure 4), with consequent strong suppression of the development of solvation forces, the disappearance of solvation force oscillations (see figure 3), and the emergence of liquid-like dynamic and response characteristics (that is, higher molecular mobilities, and continuous expulsion of molecules from the confined region in response to reduction of the gap-width, see figure 6). The different nature of the molecular films in the flat- and rough-surface confinements is portrayed also in the characteristics of the free-volumes calculated for the two systems, with that for the flat-surface confinement exhibiting local minima at gap-widths corresponding to well-layered film configurations, while in the rough-surface confinement the free-volume decreases with the gap-width in a smooth monotonic manner (see figure 5);

overall the free-volume is larger in the rough-surface confinement than in the flat-surface one, except in the vicinity of gap-widths corresponding to intermediate configurations between well-layered states of the film in the flat-surface confinement.

When the rough-surface boundaries are set in motion (at a high shear rate) the above characteristics of the confined film maintain, with the interfacial layer of the film sticking to the adjacent solid boundaries (on the two sides of the confinement gap), resulting in partial slip inside the film (see figure 7) and development of shear stress in the viscous molecular fluid (unlike the case of flat boundaries where the confined film slips at the solid boundaries resulting in a vanishingly small shear stress in the film, see figure 8). The effective viscosities calculated for the film in the rough-surface confinement are found to depend exponentially on the reciprocal of the (per molecular segment) free-volume in the confinement.

Analysis of our results shows that one of the main effects of the rough-surface morphology on the properties of the confined films is the frustration of ordering in the film. This observation, and its apparent relation to the principle of frustration of ordering that underlies our recently proposed method for friction control in lubricated junctions through externally applied small amplitude oscillations of the gap-width [5], suggests that morphological patterning of surfaces could provide ways for controlled modifications of frictional processes in thin-film lubricated nanotribological systems.

Finally, we comment on the relation between the results of our studies and investigations of issues pertaining to the effect of roughness on the boundary conditions used in modeling fluid flows past surfaces [20–25]. Molecular dynamics investigations of simple fluids (modeled as Lennard-Jones spherical particles) sheared by flat crystalline surfaces, have shown that the boundary conditions at the fluid-to-surface interface are controlled by the extent that the fluid "feels" the corrugation of the surface (see [19] and citations to earlier studies therein). In the regime for which the degree of slip of the fluid with respect to the moving solid boundary is independent of the local shear rate, the velocity difference Δv between the solid and the adjacent fluid can be described [19,36] by the well-known linear Navier boundary condition [37], $\Delta v = \delta_s \dot{\gamma}$, where δ_s is a constant slip length, with the amount of slip increasing with decreasing corrugation of the surface energy (i.e., the interaction energy between the surface and the fluid particles). At higher shear rates, the Navier boundary condition breaks down as the slip length increases rapidly with $\dot{\gamma}$ (even though the fluid remains Newtonian), diverging as the shear rate approaches a critical value $\dot{\gamma}_c$ which becomes smaller as the corrugation of the surface energy decreases [16,19]; these observations can be interpreted in terms of a maximum stress (associated with the fluid-to-solid interface) that can be supported at the interface [16].

Using the above phenomenology we may restate now the results of our simulations for hexadecane films sheared by flat- and rough-surface boundaries, as follows: (1) The complete interfacial slip and small shear stresses observed in the FS simulations (see, respectively, figure 7(a) and figure 8 (c) and (d)) imply that the shear rates used in these simulations exceeded the $\dot{\gamma}_c$ value corresponding to the FS confinement (alternatively, this may be expressed as divergence of the slip length associated with the inability of the film to support shear stress above the maximum value characteristic to the FS confinement). (2) The sticking of the film boundary layers found for the RS confinement (i.e., no slip condition corresponding to vanishing of the slip length, see figure 7(b)) that is sheared at similar shear rates as the FS one, and the development of shear stress in the film (see figure 8 (a) and (b)), imply that the $\dot{\gamma}_c$ value, or alternatively the value of the maximum shear stress, characteristic to the RS confinement, is larger then that in the FS confinement.

The above influence of surface roughness on the boundary conditions at the fluid-to-solid interface may originate from several factors, including: (a) Overall increased effective interaction between the molecular fluid and the rough-surface due to higher local surface coordination of interfacial molecular segments; indeed, examination of the distributions of the interaction energies between the interfacial molecular segments and the solid surfaces for the two confinements, reveals that the one corresponding to the rough-surface is characterized by a much larger number of molecular segments strongly bound to the surface. (b) The spatially non-uniform nature of the distribution of the interaction energies between interfacial molecular segments and the underlying solid surface, resulting in a spatially non-uniform distribution of local maximum shear stresses at the interface, with consequent inhibition (disruption) of collective slip motion. (c) The influence of the local rough-surface topography on the flow patterns in the vicinity of the boundaries (i.e., the development of velocity components governed by the local geometry of the rough-surface), leading to the development of local stresses that are related to the film viscosity and result in energy dissipation. Investigations aimed at gaining a comprehensive understanding of these effects, as well as of issues pertaining to the interplay between the length scales characteristic to such systems [38] (that is, the average gap-width and the length scales associated with the surface roughness and the confined molecules), are currently underway in our laboratory.

References

[1] J. Gao, W.D. Luedtke and U. Landman, J. Chem. Phys. 106 (1997) 4309.

[2] J. Gao, W.D. Luedtke and U. Landman, J. Phys. Chem. B 101 (1997) 4013.

[3] J. Gao, W.D. Luedtke and U. Landman, Phys. Rev. Lett. 79 (1997) 705.

[4] S. Granick, A.L. Demirel, L. Cai and J. Peansky, Isr. J. Chem. 35 (1995) 75.

[5] J. Gao, W.D. Luedtke and U. Landman, J. Phys. Chem. B 102 (1998) 5033.

[6] M. Heuberger, C. Drummond and J.N. Israelachvili, J. Phys. Chem. B 102 (1998) 5038.

[7] B. Bhushan, J.N. Israelachvili and U. Landman, Nature 374 (1995) 607.

[8] M.O. Robbins and M.H. Muser, in: *Handbook of Modern Tribology*, ed. B. Bhushan (CRC Press, Boca Raton, 2000).

[9] J. Gao, W.D. Luedtke and U. Landman, Science 270 (1995) 605.

[10] U. Landman, W.D. Luedtke and J. Gao, Langmuir 12 (1996) 4514.

[11] A. Jabbarzadeh, J.D. Atkinson and R.I. Tanner, Phys. Rev. E 61 (2000) 690.

[12] J. Galle, H.L. Vortler and K.-P. Schneider, Surf. Sci. 387 (1997) 78; L.J.D. Frink and F. van Swol, J. Chem. Phys. 108 (1998) 5588.

[13] J.N. Israelachvili, *Intermolecular and Surface Forces*, 2nd Ed. (Academic Press, New York, 1992).

[14] H. Yoshizawa, Y.-L. Chen and J.N. Israelachvili, Wear 168 (1993) 161.

[15] B. Bhushan, ed., *Handbook of Modern Tribology* (CRC Press, Boca Raton, 2000).

[16] S.P. Sutton, Interfacial phenomena in bounded simple liquids, Ph.D. Thesis, School of Physics, Georgia Institute of Technology, Atlanta, GA (1991).

[17] M.J. Stevens, M. Mondello, G.S. Grest, S.T. Cui, H.D. Cochran and P.T. Cummings, J. Chem. Phys. 106 (1997) 7303, and references therein.

[18] A. Koike and M. Yoneya, J. Phys. Chem. B 102 (1998) 3669.

[19] P.A. Thompson and S.M. Troian, Nature 389 (1997) 360.

[20] K.M. Jansons, Phys. Fluids 31 (1988) 15.

[21] P. Panzer, D. Einzel and M. Liu, Physica B 165&166 (1990) 555.

[22] D. Einzel, P. Panzer and M. Liu, Phys. Rev. Lett. 64 (1990) 2269.

[23] L. Daikhin and M. Urbach, Phys. Rev. E 49 (1994) 1424.

[24] M. Urbach and L. Daikhin, Phys. Rev. B 49 (1994) 4866.

[25] B.N.J. Persson, *Sliding Friction: Physical Principles and Applications* (Springer, Heidelberg, 1998), ch. 8.6.

[26] M. Parrinello and A. Rahman, J. Appl. Phys. 52 (1981) 7182.

[27] H.J.C. Berendsen, J.P.M. Postma, A. DiNola and J.R. Haak, J. Chem. Phys. 81 (1984) 3684.

[28] M. Mondello and G. Grest, J. Chem. Phys. 103 (1995) 7185.

[29] M.W. Ribarsky and U. Landman, J. Chem. Phys. 97 (1992) 1937.

[30] T.K. Xia, J. Ouyang, M. Ribarsky and U. Landman, Phys. Rev. Lett. 69 (1992) 1967.

[31] J.B. Adams, S.M. Foiles and W.G. Wolfer, J. Mater. Res. Soc. 4 (1989) 102.

[32] J. Klein and E. Kumacheva, Science 269 (1995) 816.

[33] J. Van Alsten and S. Granick, Phys. Rev. Lett. 61 (1988) 2570; H.-W. Hu, G.A. Carson and S. Granick, Phys. Rev. Lett. 66 (1991) 2758; S. Granick, Science 253 (1991) 1374.

[34] M.H. Cohen and D. Turnbull, J. Chem. Phys. 31 (1959) 1164.

[35] J.D. Ferry, *Viscoelastic Properties of Polymers* (Wiley, New York, 1980).

[36] P.A. Thompson and M.O. Robbins, Phys. Rev. A 41 (1990) 6830.

[37] H. Lamb, *Hydrodynamics* (Dover, New York, 1932).

[38] J.R.A. Pearson and C.J.S. Petrie, in: *Polymer Systems: Deformation and Flow*, eds. R.E. Wetton and R.W. Whorlow (Macmillan, London, 1968) p. 163.